Northumbria Research Link

Northumbria
University
NEWCASTLE

UniversityLibrary

A Machine Learning Based Signal Demodulator in NOMA-VLC

Bangjiang Lin, Qiwei Lai, Zabih Ghassemlooy, *Fellow of OSA, Senior Member, IEEE* and Xuan Tang

Abstract—Non-orthogonal multiple access (NOMA) is a promising scheme to improve the spectral efficiency, user fairness, and overall throughput in visible light communication (VLC) systems. However, the error propagation problem together with linear and nonlinear distortions induced by multipath, limited modulation bandwidth, and nonlinearity of light emitting diode significantly limit the transmission performance of NOMA-VLC systems. In addition, having an accurate channel state information, which is important in the recovery of the NOMA signal, in mobile wireless VLC is challenging. In this work, we propose a convolutional neural network (CNN)-based demodulator for NOMA-VLC, in which signal compensation and recovery are jointly realized. Both simulation and experiment results show that, the proposed CNN-based demodulator can effectively compensate for both linear and nonlinear distortions, thus achieving improved bit error ratio performance compared with the successive interference cancellation and joint detection-based receivers. Compared to SIC, the performance gains are 1.9, 2.7, and 2.7 dB for User1 for the power allocation ratios (PARs) of 0.16, 0.25, and 0.36, respectively, which are 4, 4, and 2.6 dB for User2 for PARs of 0.16, 0.25, and 0.36, respectively.

Index Terms—**visible light communications (VLC), non-orthogonal multiple access (NOMA), convolutional neural network (CNN).**

I. Introduction

Visible light communications (VLC) is one of the possible contenders for short range communications and local area networks in the fifth generation networks [1]. Multiple access technologies can increase the data rates and reduce the cost significantly, thus contributing to the implementation and commercialization of VLC systems in a range of applications in indoor environments. To date, the used multiple access schemes in cellular networks are based on orthogonal multiple access (OMA) schemes including frequency division multiple access (FDMA), time division multiple access, code division multiple access, and orthogonal frequency division multiple access (OFDMA), in which users are allocated with orthogonal resources (i.e., distinct frequency channels, time slots, and signature codes). The orthogonality feature ensures low levels of interference between user at the cost of imposing the upper limit on the number of supported users, achievable data rate and spectral efficiency. Recently, non-orthogonal multiple access (NOMA)-based schemes have attracted considerable attentions from academia, industry and standardization bodies (i.e., the 3rd generation partnership project) due to their improved spectral efficiency and user fairness, low transmission latency, and higher cell-edge throughputs [2-6].

Application of NOMA in VLC systems have been widely reported [7]. In [8], NOMA was shown to be particularly suitable for VLC due to high signal to noise ratio (SNR), whereas in [9-11], it was shown that for VLC downlinks NOMA could achieve improved transmisison performance (such as higher sum rates for a larger number of users) compared with OMA. Effective power allocation methods for NOMA-VLC have been extensively investigated in the litrature [8, 12-13]. In [8], a gain ratio power allocation (GRPA) strategy that considered users' channel conditions to ensure efficient and fair power allocation was proposed, whereas in [12] optimal power allocation schemes for both static and mobile users were proposed. In [13], a user grouping and power allocation method was proposed for NOMA-VLC multi-cell networks and in [14] a downlink power allocation scheme was proposed to achieve a flexible tradeoff between the sum rate and user fairness. The experimental demonstration of NOMA-VLC links with higher system capacity were reported in [15-18]. In [15], a bidirectional NOMA-OFDMA VLC link with dynamic bandwidth allocation and higher system capacity for a larger number of users was experimentally investigated. In [16], a phase pre-distortion method to improve the symbol error rate performance of an uplink NOMA-VLC system was proposed and experimentally demonstrated. In [17], an offset quadrature amplitude modulation (OQAM)/OFDM combined with NOMA was proposed and experimentally demonstrated in a multi-user and asynchronous multi-cell VLC system. In [18], a real-time software reconfigurable dynamic power-and-subcarrier allocation scheme for OFDM-NOMA VLC was proposed and expeimenatlly investigated. In addtion, the use of NOMA in multiple inputs multiple outputs VLC were reported in [19, 20].

In NOMA-VLC systems, there are two issues: (*i*) error propagation (EP) due to the use of successive interference cancellation (SIC)-based receiver (Rx) for decoding the multiplexed signal [21]; (*ii*) link performance being susceptible

Bangjiang Lin (linbangjiang@fjirsm.ac.cn), Qiwei Lai and Xuan Tang are with Quanzhou Institute of Equipment Manufacturing, Haixi Institutes, Chinese Academy of Sciences, Quanzhou, China. Zabih Ghassemlooy is with Optical Communications Research Group, Faculty of Engineering and Environment, Northumbria University, NE1 8ST, Newcastle, U.K. (e-mail: z.ghassemlooy@northumbria.ac.uk). Corresponding author: Xuan Tang (xtang@fjirsm.ac.cn).

to multipath induced linear and nonlinear distortions, limited modulation bandwidth B_{LED} and nonlinearity of LEDs, etc. A SIC-free NOMA scheme was proposed in [22] to mitigate the EP, thus improving the user's fairness and the bit error rate (BER) performance. To mitigate the linear and nonlinear distortions, accurate channel state information (CSI) is required, which is challenging to achieve under the user's mobility and driving bias drift. The channel estimation (CE) technologies adopted in radio frequency (RF)-based communication systems, such as pilot adied CE may also be applicable to VLC, but suffer from a notable residual error floor and not adapting to CSI variations [23-24]. As shown in [15], the CE error degraded the link performance. However, linear and hybrid equalizers based on an adaptive finite impulse response (FIR) filter with and without Volterra series and look-up table schemes, respectively have been widely studied to mitigate the linear and nonlinear distortions in VLC systems [25-28]. In [29], a singular value decomposition-based Chebyshev precoding method was proposed for nonlinear compensation in NOMA-VLC.

Recently, machine learning (ML) techniques especially the neural networks (NNs) have been introduced in VLC to make them become more efficient by addressing many problems in the physical layer. In [30] and [31], a clustering algorithm-based perception decision method and a nonlinear compensation scheme based on K-means clustering algorithm were proposed for multi-cap and Nyquist pulse amplitude modulation (PAM) VLC systems, respectively. In [32], a memory controlled deep long short-term memory (LSTM)-based post-equalizer was proposed to mitigate transmission impairments in PAM-VLC. In [33], a deep-learning (DL)-based multi-colored VLC link using red, green, and blue LEDs was reported. In [34], the design and implementation of a VLC link with ML-based signal demodulation method was investigated.

In this work, we propose a convolutional NN (CNN)-based signal demodulator to mitigate both linear and nonlinear distortions in NOMA-VLC. The captured NOMA signals are (*i*) used to train the CNN in the offline mode; and (*ii*) directly applied to the CNN-based demodulator for signal compensation and recovery in the online mode. Note that, there is no need for the free-space channel response in detecting the NOMA signal. Using simulation and experiment results, we show that the proposed CNN-based demodulator can effectively mitigate linear and nonlinear distortions, thus improving the system performance.

The rest of the paper is organized as follows. Section II describes the proposed CNN-based demodulation method in detail. Section III presents the simulation setup and results for the CNN-based NOMA-VLC system. Section IV presents the experiment setup and results for the CNN-based NOMA-VLC system followed by the concluding remarks in Section V.

II. CNN-BASED SIGNAL DEMODULATION METHOD

Figure 1 shows the schematic diagram of NOMA-VLC with a CNN-based demodulator. At the transmitter (Tx), the data streams from the source data modules mapped into 4-quadrature amplitude modulation (QAM) are applied to the OFDM modulators, the output of which are passed through

power allocation modules prior to being combined. The generated NOMA signal is direct current (DC) biased prior to
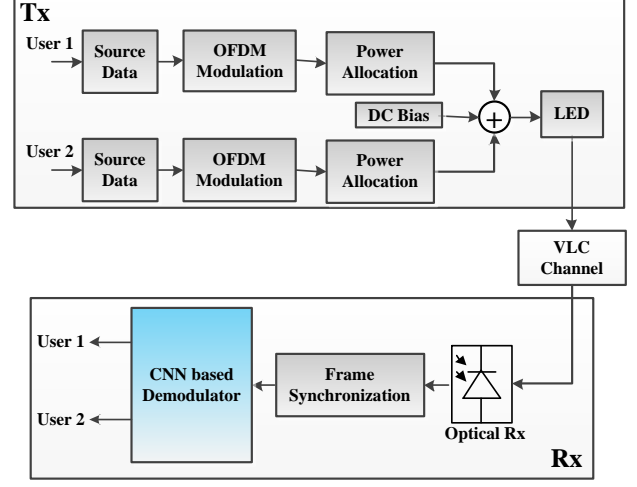

Fig. 1. Block diagram of NOMA-VLC system employing a CNN-based demodulator.

intensity modulation (IM) of the LED. Following free space transmission, the optical NOMA signal is detected using an optical Rx (i.e., a photodiode (PD) and a transimpedence amplifier), the output of which is given by:

$$y = \gamma P_t h + w, \qquad (1)$$

where γ is the responsibility of the PD, P_t is the transmit optical power, and w is the additive white Gaussian noise (AWGN), which is the sum of contributions from the shot noise (induced by the signal and the ambient light) and the thermal noise. h is the channel gain from LED to the optical Rx as given by:

$$h = \frac{(m_L + 1)A_{PD}}{2\pi d^2} TG \cos^{m_L}(\varphi) \cos(\theta), \qquad (2)$$

where m_L is Lambertian emission order, A_{PD} is the active area of the PD and d is the distance between the LED and the PD. T and G are the gains of the filter and lens at the Rx, respectively. φ and θ are the emission and the incident angles, respectively. Note, the optical gain will be zero if the incident light is outside the Rx's field of view. Following optical detection, the regenerated electrical NOMA signal is applied to the frame synchronization module. Note, at the Tx we have inserted two Chu sequences in each frame header of the NOMA signal. At the Rx, following correlation operation the frame head is readily detected and following frame synchronization the NOMA signal is decoded directly using the CNN-based demodulator, where distortion compensation and signal demapping are jointly realized. In the SIC-based Rx, each user will decode its own message following decoding of the messages from relatively weaker users U_w (i.e., allocated with higher power), while treating messages from the stronger users U_s (i.e., allocated with lower power) as the noise signal. In the meanwhile, for U_w the decoded messages are subtracted from the received signal. However, if the message of U_w cannot be decoded without an error, the generated error will propagate to U_s, which is known as the EP problem. In addition, in SIC-based Rxs accurate channel estimation is a requirement to

achieve an improved performance. Note, in VLC systems with the user's mobility and driving bias drift, it becomes challenging to obtain the channel responses. In this work, the minimum mean square error (MMSE)-based CE [15] is used to calculate the CSI in the SIC-based Rx, which performs better than other conventional CE methods. However, the transmission performance is affected by high correlation among the channel responses of users due to the lack of small-scale effects when the transmit precoding schemes are applied. In the proposed CNN based demodulator, we have performed channel equalization implicitly with signal demodulation, therefore it suffers from less influence from the high correlation among the channel responses of users. In addition, no pilot overhead and CSI is required in CNN based Rx.
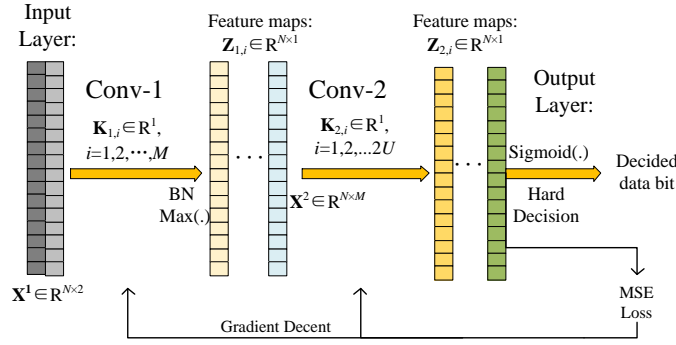

Fig. 2. The structure of CNN-based demodulator.

Figure 2 shows the structure of the CNN-based demodulator, which comprises of the input layer, two convolutional layers, and output layer. The input layer with a dimension of $N \times 2$ corresponds to the real and imaginary parts of signals modulated on N-subcarrier (i.e., $\mathbf{X}^R$ and $\mathbf{X}^I$). In the first convolutional layer (Conv-1), $\mathbf{X}^1 = [\mathbf{X}^R, \mathbf{X}^I]$ convolutes with M-kernel, the output of which is given as:

$$\mathbf{Y}_i^1 = \mathbf{X}^1 * \mathbf{K}_{1,i} + b_{1,i}, \qquad (3)$$

where $\mathbf{K}_{1,i}$ denotes the i-th kernel of Conv-1, $i = 1, 2, …, M$ and $b_{1,i}$ is the bias of $\mathbf{K}_{1,i}$. To prevent overfitting and improve the training speed as well as speed-up the convergence process, we have added batch normalization (BN), which can be expressed as:

$$x_{BN} = \frac{x - \mathrm{E}[x]}{\sqrt{\mathrm{Var}[x] + \varepsilon}} * \gamma + \beta, \qquad (4)$$

where x is the input, x_{BN} is the normalized output, and β and γ are the learnable parameters. The activation function of the convolutional layer is the leaky rectified linear unit (Relu), which is a piecewise linear function performing a threshold operation, where any input value less than zero is multiplied by a fixed scalar. Relu has been adopted as the default activation function in many types of NNs because it is easier to train and often achieves improved performance. The final output of Conv-1 is given as:

$$\mathbf{Z}_{1,i} = \max(0, \mathrm{BN}(\mathbf{Y}_i^1)). \qquad (5)$$

The input of the 2nd convolutional layer (Conv-2) is $\mathbf{X}^2 = [\mathbf{Z}_{1,1}, \mathbf{Z}_{1,2}, …, \mathbf{Z}_{1,M}]$. Conv-2 contains $2U$-kernel (i.e., $\mathbf{K}_{2,i}$, $i = 1, 2, …, 2U$), where U is the number of users. $\mathbf{X}^2$ is first convoluted with $\mathbf{K}_{2,i}$ as follow:

$$\mathbf{Y}_i^2 = \mathbf{X}^2 * \mathbf{K}_{2,i} + b_{2,i}, \qquad (6)$$

where $b_{2,i}$ is the bias of $\mathbf{K}_{2,i}$. Sigmoid function is used as the output activation function, and the final output of Conv-2 is given as:

$$\mathbf{Z}_{2,i}(j) = \mathrm{sigmoid}\left(\mathbf{Y}_i^2(j)\right). \qquad (7)$$

Note, as for the non-linearity there are several options, with the simplest being the threshold operation, which is adopted here. Thus, if $\mathbf{Z}_{2,i}(j) > 0.5$, the received i-th data bit on the j-th subcarrier is 1, otherwise it is 0. There are many functions, which could be used to estimate the error of a set of weights in NNs. A loss function is chosen in determining the error of the model during the optimization process, which is defined as the MSE. The network is trained with backpropagation and gradient descent with Rmsprop optimization. In general, NNs with more hidden layers or more network nodes per layer are potentially more powerful to express complex functions at the cost of increased computation complexity [35]. In addition, simple NNs would perform better than complex NNs in solving relatively simple problems [35]. In the convolutional layers, we have adopted a higher number of kernels, but with the reduced size for the ease of computation complexity. We have verified that, increasing the number of convolutional layers and the size of kernel will not improve the performance of NN-based demodulator as shown in the simulation results. Note, other NNs, such as fully connected NN (FNN), LSTM network, and hybrid networks (e.g., one convolutional layer plus one FNN) can also be used to decode the NOMA signal. However, the convergence speed of LSTM is much slower compared with the FNNs and CNNs. Due to its characteristic of sparse connections and weight sharing, convolutional layer-based NNs can use fewer training parameters to achieve the same performance compared with FNNs [36]. As such, convolutional layer-based NNs have the advantages of lower complexity, higher convergence speed and improved optimization of the network model, thus being adopted as the decoder in this work. In addition, we have verified that LSTM and FNN cannot achieve improved performance compared with the convolutional layer-based NNs as shown in the simulation results.
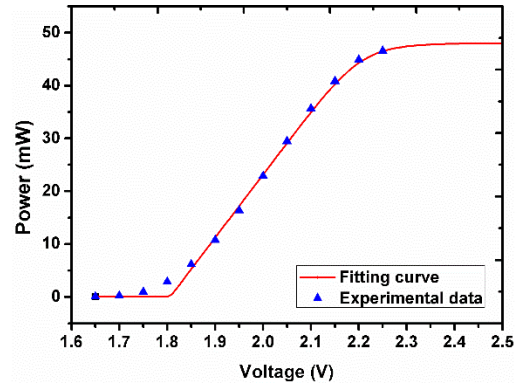

Fig. 3. *P-U* characteristic of the LED.

III. SIMULATION RESULTS

In this section, we investigate the transmission performance of the proposed CNN-based Rx using Matlab and Python. At the Tx as shown in Fig. 1, two random binary data streams are converted into 4-QAM symbols prior to generation of OFDM signals. The sizes of inverse discrete Fourier transform (IDFT) and the cyclic prefix (CP) are 64 and 6, respectively. Note, the baseband OFDM signals are up-converted to a 3.75 MHz radio frequency (RF) carrier signal to ensure that OFDM signals are real. For OFDM signals the Baud rates are 5 M. Next, the two OFDM signals with different power levels are combined and DC-biased prior to IM of the LED. Note, the transmission performance of VLC systems is affected by the frequency response (i.e., B_{LED}) and the power-voltage (P-U) characteristic of the LED, see Fig. 3. In the simulation, we have assumed that, B_{LED} is about 10 MHz. Here, we have used the experimental sampling data to fit the P-U curve, which can be expressed as:

$$P_t = \begin{cases} 0 & U < \dfrac{b}{a} \\ \dfrac{aU - b}{(1 + (\dfrac{aU - b}{P_{max}})^k)^{\frac{1}{k}}} & U >= \dfrac{b}{a} \end{cases} , \qquad (8)$$

where a, b, k and P_{max} are the fitting parameters, which are set to 119.17, 215.18, 10, and 48 mW, respectively. As shown in Fig. 3, the linear range is from 1.85 to 2.2 V, beyond which the transmitted signal will experience clipping (i.e., nonlinear distortion), which is more problematic in OFDM-based NOMA with a high peak to average power ratio. Following transmission over the free space channel, an optical Rx is used to regenerate the electrical NOMA signal for further processing. The NOMA signal is first frame synchronized and then down-converted to the baseband signal. Following CP removal, the NOMA signal is converted back to the frequency domain using discrete Fourier transform (DFT). The CNN-based demodulator is then used to decode the NOMA signal directly. In the simulation, both data sets for offline training and online deployment are generated randomly using the random function of Matlab, so that the proposed NN-based Rx is unable to characterize the random sequences used [37]. Here, we have used data sets of 128000- and 128000-bit for training and testing, respectively. Finally, the performance of the link is evaluated in terms of the BER. All the key system parameters are provided in Table I.

TABLE I. SIMULATION PARAMETERS

Parameter	Value
• Modulation bandwidth of LED • Power allocation ratios • Number of users	10 MHz 0.16, 0.25, 0.36 2
NOMA-OFDM • DFT • CP • RF carrier frequency • Symbol rate • Modulation format • Total bit rate	 64 6 3.75 MHz 5 M 4-QAM 18.3 Mbps

Table II shows the BER performances as a function of the kennel size with power allocation ratio (PAR) of 0.25 under the received signal to noise ratio (SNR) of 13. The DC bias and the

peak to peak voltage V_{pp} of the driving signal are set to 2.1 and 0.6 V, respectively. The numbers of kernel in Conv-1 and Conv-2 are set to 64 and 4, respectively. As shown in Table II, the best kernel size is 1×2 considering the BER performance and complexity of CNN. Table III shows the BER performances as a function of the number of convolutional layer with the PAR of 0.25 under the received SNR of 13. The DC bias and tV_{pp} of the driving signal are set to 2.1 and 0.6 V, respectively. The number of kernels for the last convolutional layer and other layers are 4 and 64, respectively. The BER performances do not improve as the number of convolutional layer increases, but the complexity of CNN significantly increases. Based on the above simulation investigations, the kernel size and the number of convolutional layer are set to 1×2 and 2, respectively considering the BER performance and the complexity of NN.

TABLE II. BER PERFORMANCE VERSUS KERNEL SIZE

Kernel size	BER of User1	BER of User2	Average BER
1×2	1.2e-5	7.3e-5	4.3e-5
2×2	0	9.2e-5	4.6e-5
3×2	0	1e-4	5e-5

TABLE III. BER PERFORMANCE VERSUS CONVOLUTIONAL LAYER NUMBER

Layer number	BER of User1	BER of User2	Average BER
2	1.2e-5	7.3e-5	4.3e-5
3	1.3e-5	7.3e-5	4.3e-5
4	1.2e-5	7.6e-5	4.4e-5

TABLE IV. COMPLEXITY COMPARISON FOR CNN, FNN AND LSTM

Network Type	CNN	FNN	LSTM
Number of parameters	$3M+2MU+2U$	$2N(M+UM+U)+M$	$4(M^2+3M+4U^2+2UM+2U)$
Complexity of Network	$(2U+2)NM$	$2NM(U+1)$	$N(4M^2+11M+16U^2+8UM+6U)$

M is the number of kernel of Conv-1 for CNN, or the number of nodes in the hidden layer for LSTM and FNN. U is the number of users and N is the number of subcarriers.
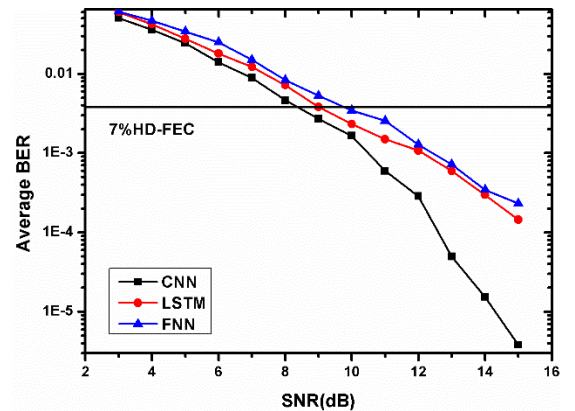

Fig. 4 BER performance comparison for CNN, FNN, and LSTM.

FNN and LSTM networks are also considered here. The comparison of BER performances and complexities with the PAR of 0.25 for CNN, FNN, and LSTM are shown in Fig. 4

and Table IV, respectively. The DC bias and V_{pp} of the driving signal are set to 2.1 and 0.6 V, respectively. The numbers of hidden layer for FNN and LSTM are both 1, which contains M nodes ($M = 64$). As shown in Table IV are the expression for the number of parameters and the computational complexity of LSTM, FNN and CNN. As shown in Fig. 4, CNN offers improved performance than both FNN and LSTM particularly at higher values of SNR.
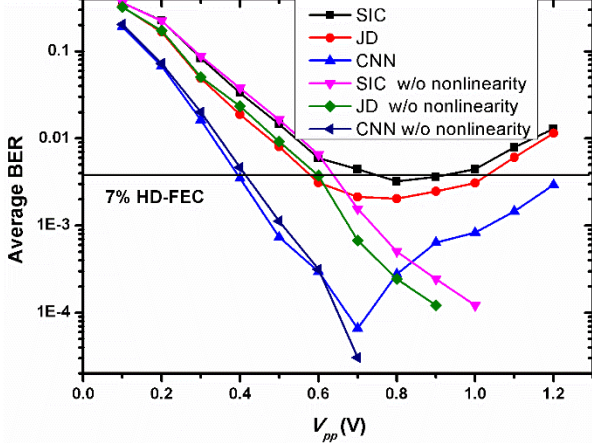

Fig. 5. The BER performances with and without nonlinear distortion for SIC, JD, and CNN-based Rxs for PAR of 0.25.

As part of efficiency evaluation of the proposed CNN-based Rx, we have considered the SIC and joint detection (JD)-based Rx for comparison. The JD algorithm can be expressed as:

$$\{\hat{x}_1, \hat{x}_2\} = \arg\max_{\{x_1, x_2\}} \text{Prob}(y/x_1, x_2), \qquad (9)$$

where ($\hat{x}_1, \hat{x}_2$) is the detected signal-pair output by the JD algorithm. JD is a maximum-likelihood (ML) estimation method, which performs better than SIC at the cost of higher computational complexity [38]. The computational complexity to decode the NOMA signal in (9) is $N \times 4^U$. Note, channel estimation and equalization is also required for JD-based Rx. Fig. 5 show the average BER performance as a function of V_{pp} for the PAR of 0.25. The noise power in (1) is 32 dBm. Both JD and CNN-based Rx show improved BER performances compared with the SIC-based Rx. With no nonlinear distortion, the BER performances improves with increasing V_{pp}, because of increasing SNR. With nonlinear distortion, the BER improves with V_{pp}, reaching the minimum values at V_{pp} of 0.8, 0.7, and 0.7 V for SIC, JD, and CNN, respectively, beyond which the BER increases due to nonlinear distortions. Note, OFDM can effectively combat the linear distortion, thus the BER performances with and without nonlinear distortion are similar at lower V_{pp}. Fig. 6 shows the BER performance as a function of the received SNR for V_{pp} of 0.6V, and a range of power allocation ratios (PARs) of 0.16, 0.25, and 0.36 for CNN, JD, and SIC-based Rxs, respectively. For the PAR of 0.16, the required SNRs to achieve a BER of 3.8e-3 are about 6.6, 6.3, and 4.7 dB for User1 for SIC, JD, and CNN, respectively, which are 14, 13, and 10 dB for User2 for SIC, JD, and CNN, respectively. Compared with SIC, the performance gains are 0.3 and 1.9 dB for User1 for JD and CNN, respectively, which are 1 and 4 dB for User2 for JD and CNN, respectively. With the PAR of 0.25, the required SNRs to achieve a BER of 3.8e-3 are

about 9.3, 8.5, and 6.6 dB for User 1 for SIC, JD, and CNN, respectively, which are 12, 11.6, and 8.1 dB for User2 for SIC, JD, and CNN, respectively. Thus, for Users 1 and 2 the performance gains are 0.8 and 2.7 dB; and 0.4 and 3.9 dB for JD and CNN, respectively. For the PAR of 0.36 and for Users 1 and 2, the required SNRs are {12, 11.2, and 9.3 dB} and {12.6, 12.3, and 10 dB} for JD and CNN, respectively.
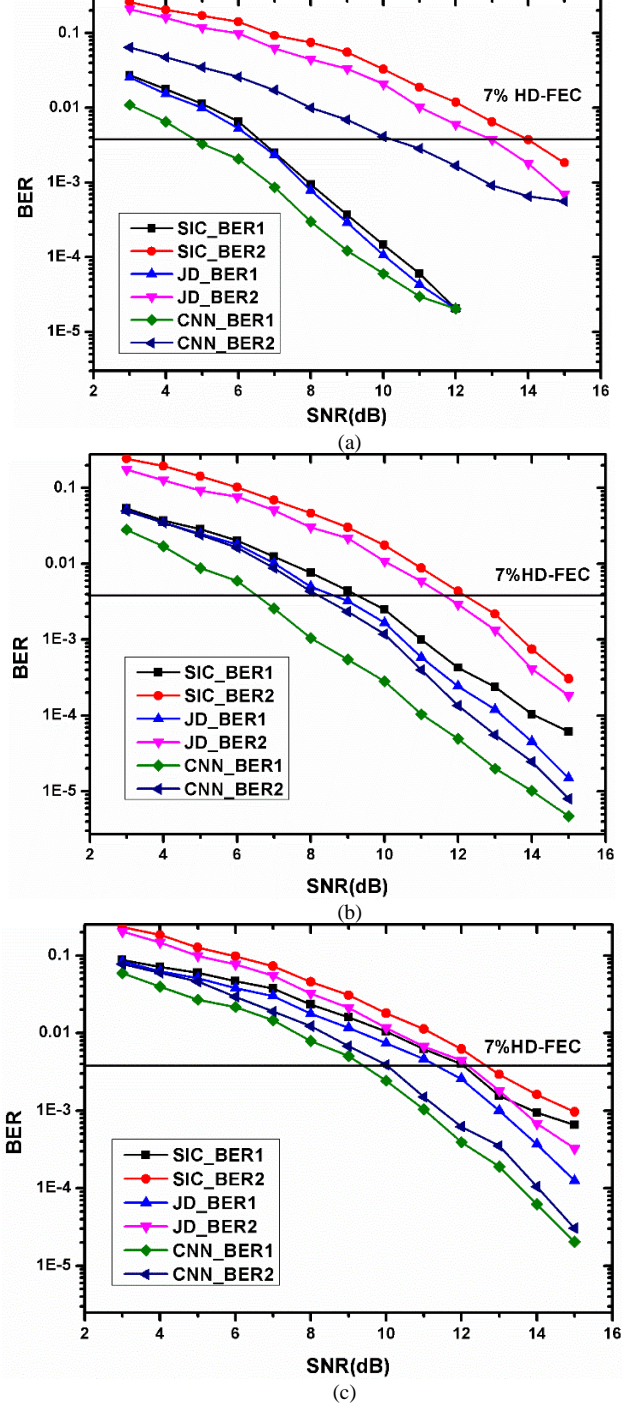

(a)

(b)

(c)

Fig. 6. The BER performance as a function of SNR for the SIC, JD, and CNN-based Rxs for PAR of: (a) 0.16, (b) 0.25, and (c) 0.36.

TABLE V. SNR @ BER OF 3.8e-3

		SIC	JD	CNN
PAR=0.16	User1	6.6 dB	6.3 dB	4.7dB

	User2	14 dB	13 dB	10 dB
PAR=0.25	User1	9.3 dB	8.5 dB	6.6 dB
	User2	12 dB	11.6 dB	8 dB
PAR=0.36	User1	12 dB	11.2 dB	9.3 dB
	User2	12.6 dB	12.3 dB	10 dB

. So the performance gains for JD and CNN are 0.8 and 2.7 dB, and 0.3 and 2.6 dB for Users 1 and 2, respectively. The results indicate that, the proposed CNN-based Rx can effectively compensate for both the linear and nonlinear distortions, thus improving the BER performances compared with the SIC and JD-based Rxs. All the key simulation results are summarized as shown in Table V.
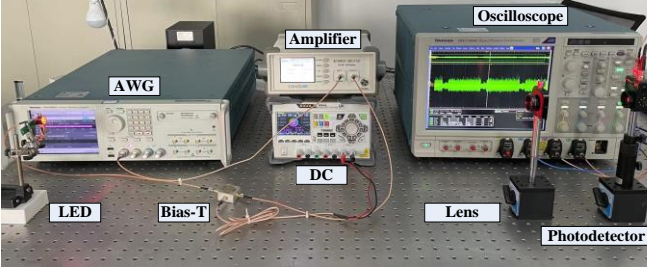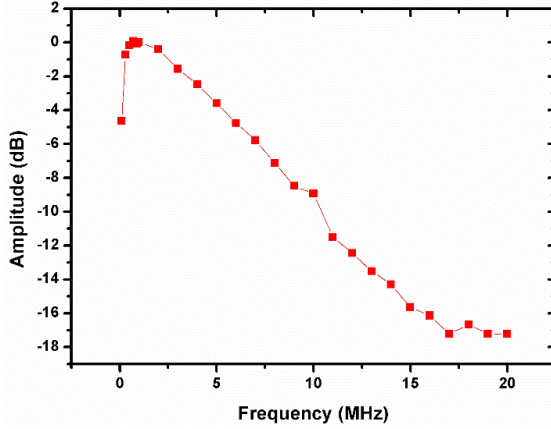

Fig. 7. Experiment setup for CNN-based NOMA-VLC.

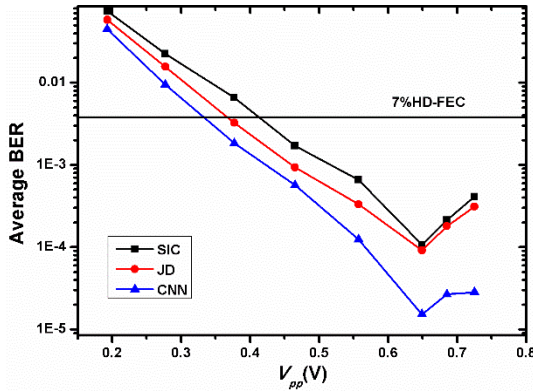
Fig. 8. Frequency response of the VLC system.

Fig. 9. The measured BER as a function of V_{pp} for the CNN, JD, and SIC-based Rxs.

IV. EXPERIMENT SETUP AND RESULTS

In this section, we evaluate the performance of the CNN-based Rx by experimental investigation using the setup shown in Fig. 7. At the Tx, the generated baseband NOMA signal with two users is up sampled by three and then up-converted to a RF carrier via digital I-Q modulation. This ensures the NOMA signal being real value for IM of the LED. The frequency response of the LED in the low frequency (0-1MHz) is not good as shown in Fig. 8. The NOMA signal would suffer from less distortion after up-conversion. The sizes of IDFT and the CP are 64 and 6, respectively. The modulation format is 4-QAM for each user. The digital NOMA signal is uploaded onto an arbitrary waveform generator (Tektronix AWG 70002A), the output of which is applied to an amplifier with a gain of 20 dB. The NOMA signal is DC biased using a bias tee prior to IM of a phosphorescent red LED having a 10-dB bandwidth of ~10 MHz, see Fig. 8. At the Rx, a lens is used to focus the optical signal into the optical Rx (THORLABS PDA36A), which is composed of a PIN PD and a transimpedance amplifier, with a responsivity of 0.65 A/W, gain of 0.75×10^3 V/A and NEP of 7.7×10^{11} W/Hz$^{0.5}$. The regenerated NOMA signal is captured using a real-time digital oscilloscope (DPO 71604) for further offline processing. The detected NOMA signal is decoded using the proposed CNN, SIC and JD-based demodulators. Note, we have used a data set of 64000-bit for both training and testing.

Fig. 9 shows the average BER performances as a function of V_{pp} of the driving signal for IM of the LED for CNN, JD, and SIC-based Rxs. The distance between the Tx and the Rx is 1 m and the total data rate R_b is 13.3 Mb/s. The DC bias is 2.1 V and the PAR is 0.25. As shown in Fig. 3, the signal suffers from high nonlinear distortion outside the range of 1.8 to 2.4 V (i.e., V_{pp} of 0.6 V). We can observe that, the BER improves with V_{pp}, reaching the minimum values at V_{pp} of 0.65 V for all the Rxs, beyond which the BER increases due to nonlinear distortions. The experimental results coincide with the simulation results shown in Fig. 5. The proposed CNN-based Rx outperform the SIC and JD-based Rxs due to its improved robustness against both linear and nonlinear distortions.

Fig. 10 shows the BER performances as a function of R_b for CNN, JD, and SIC-based Rxs. The distance between the Tx and the Rx is 1.2 m and the PAR is 0.25. The DC bias and V_{pp} of the driving signal are 2.1 and 0.65 V, respectively. At the BER of 3.8e-3, the achievable R_b are 20.6, 21.4, and 24.9 Mbps for User1 for SIC, JD, and CNN-based Rxs, respectively, which are 6, 11, and 19.4 Mbps for User2 for SIC, JD and CNN, respectively. Therefore, compared with the SIC-based Rx, the proposed CNN-based Rx can increase R_b by up to 323 and 121% for User2 and User1, respectively. It should be pointed out that, it is challenging to increase the modulation format order and the number of multiplexing layer in the power domain due to the limited SNR in practical applications. To increase the number of users, we can combine the NOMA scheme with OMA schemes, such as OFDMA so that each user can utilise all the subcarrier frequencies or a set of subcarriers to transmit its data. The users with similar channel gains from the Tx to the Rx are allocated in the same power domain layer, otherwise they are allocated in different power domain layers.

IV. CONCLUSION

For the first time, we investigated the ML-based signal demodulation method in NOMA-VLC for joint signal compensation and recovery. We showed that, using offline training of NN channel characteristics and signal mapping could be achieved simultaneously. We carried out both simulation and experiment investigations to demonstrate the feasibility of the proposed CNN-based Rx in NOMA-VLC. Results showed that, the proposed CNN-based Rx could effectively compensate for both the linear and nonlinear distortions induced by multipath dispersion, limited modulation bandwidth and nonlinearity of LEDs, thus offering improved transmisison perofrmance compared with SIC and JD-based Rxs. Compared with the SIC-based Rx, the performance gains were 1.9, 2.7 and 2.7 dB for User1 for PARs of 0.16, 0.25, and 0.36, respectively increasing by 2.1, 1.3, and 0 dB for User2 for the same PARs, respectively. For the PAR of 0.25, the increased data rates at the 7% FEC BER limit were 4.3 and 13.4 Mbps for User1 and User2, respectively.
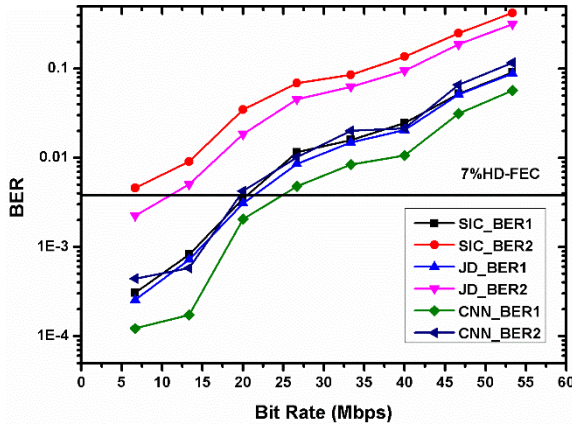

Fig. 10. The measured BER as a function of data rate for the CNN, JD, and SIC-based Rxs.

REFERENCES

1. Z. Ghassemlooy, W. Popoola, and S. Rajbhandari, *Optical Wireless Communications: System and Channel Modelling With MATLAB*. Boca Raton, FL, USA: Taylor & Francis, 2012.
2. L. Dai, B. Wang, Z. Ding, Z. Wang, S. Chen, and L. Hanzo, "A survey of non-orthogonal multiple access for 5G," *IEEE Communications Surveys & Tutorials*, vol. 20, no. 3, pp. 2294–2323, 3rd Quarter 2018.
3. Y. Chen, A. Bayesteh, Y. Wu, B. Ren, S. Kang, S. Sun, Q. Xiong, C. Qian, B. Yu, Z. Ding, S. Wang, S. Han, X. Hou, H. Lin, R. Visoz, and R. Razavi, "Toward the standardization of non-orthogonal multiple access for next generation wireless networks," *IEEE Communications Magazine*, vol. 56, no. 3, pp. 19–27, Mar. 2018.
4. M. Vaezi, Z. Ding, and H. V. Poor, *Multiple Access Techniques for 5G Wireless Networks and Beyond*. Springer: Berlin, Germany, 2019.
5. M. Vaezi, R. Schober, Z. Ding, and H. V. Poor, "Non-orthogonal multiple access: Common myths and critical questions," *IEEE Wireless Communications*, vol. 26, no. 5, pp. 174–180, Oct. 2019.
6. S. R. Islam, N. Avazov, O. A. Dobre, and K.-S. Kwak, "Power-domain non-orthogonal multiple access (NOMA) in 5G systems: Potentials and challenges," *IEEE Communications Surveys & Tutorials*, vol. 19, no. 2, pp. 721–742, 2nd Quarter 2017.
7. Hanaa Marshoud, Sami Muhaidat, Paschalis C. Sofotasios, Sajjad Hussain, Muhammad Ali Imran, Bayan S. Sharif, "Optical Non-Orthogonal Multiple Access for Visible Light Communication," *IEEE Wireless Communications*, vol. 25, no. 2, pp. 82-88, April 2018.
8. H. Marshoud, V. M. Kapinas, G. K. Karagiannidis, and S. Muhaidat, "Non-orthogonal multiple access for visible light communications,"

9. *IEEE Photon. Technol. Lett.*, vol. 28, no. 1, pp. 51–54, Jan. 1, 2016.
9. L. Yin, W. O. Popoola, X. Wu, and H. Haas, "Performance evaluation of non-orthogonal multiple access in visible light communication," *IEEE Trans. Commun.*, vol. 64, no. 12, pp. 5162–5175, Dec. 2016.
10. R. C. Kizilirmak, C. R. Rowell, and M. Uysal, "Non-orthogonal multiple access (NOMA) for indoor visible light communications," in *Proc. IEEE Int. Workshop Opt. Wireless Commun.*, 2015, pp. 98–101.
11. H. Marshoud, P. C. Sofotasios, S. Muhaidat, G. K. Karagiannidis, B. S. Sharif, "On the performance of visible light communication systems with non-orthogonal multiple acces," *IEEE Trans. on Wirel. Commun.* vol. 16 , no. 10 , pp. 6350 – 6364, Oct. 2017.
12. Shuai Ma, Yang He, Hang Li, Songtao Lu, Fan Zhang, Shiyin Li, "Optimal Power Allocation for Mobile Users in Non-Orthogonal Multiple Access Visible Light Communication Networks," *IEEE Transactions on Communications*, vol. 67, no. 3, pp. 2233 – 2244, March 2019.
13. X. Zhang, Q. Gao, C. Gong, and Z. Xu, "User grouping and power allocation for NOMA visible light communication multi-cell networks," *IEEE Commun. Lett.*, vol. 21, no. 4, pp. 777–780, Apr. 2017.
14. Zanyang Dong, Tao Shang, Qian Li, and Tang Tang, "Differential evolution-based optimal power allocation scheme for NOMA-VLC systems," *Opt. Exp.*, vol. 28, no. 15, pp. 21627-21640, 2020.
15. B. Lin, W. Ye, X. Tang, and Z. Ghassemlooy, "Experimental demonstration of bidirectional NOMA-OFDMA visible light communications," *Opt. Exp.*, vol. 25, no. 4, pp. 4348–4355, 2016.
16. X. Guan, Y. Hong, Q. Yang, and C. C.-K. Chan, "Non-orthogonal multiple access with phase pre-distortion in visible light communication," *Opt. Exp.*, vol. 24, no. 22, pp. 25816–25823, 2016.
17. Jin Shi, Jing He, Kaiquan Wu, Jie Ma, "Enhanced Performance of Asynchronous Multi-Cell VLC System Using OQAM/OFDM-NOMA," *Journal of Lightwave Technology*, vol. 37, no. 20, pp. 5212 – 5220, Oct.15, 2019.
18. Jin Shi, Yang Hong, Rui Deng, Jing He, Lian-Kuan Chen, Gee-Kung Chang, "Demonstration of Real-Time Software Reconfigurable Dynamic Power-and-Subcarrier Allocation Scheme for OFDM-NOMA-Based Multi-User Visible Light Communications," Journal of Lightwave Technology, vol. 37, no. 17, pp. 4401 – 4409, 2019.
19. B. Lin, Z. Ghassemlooy, X. Tang, Y. Li, and M. Zhang, "Experimental demonstration of optical MIMO NOMA-VLC with single carrier transmission," *Opt. Commun.*, vol. 402, pp. 52–55, Nov. 2017.
20. C. Chen, W.-D. Zhong, H. Yang, and P. Du, "On the performance of MIMO-NOMA-based visible light communication systems," *IEEE Photon. Technol. Lett.*, vol. 30, no. 4, pp. 307–310, Feb. 15, 2018.
21. H. Li, Z. Huang, Y. Xiao, S. Zhan, and Y. Ji, "Solution for error propagation in a NOMA-based VLC network: symmetric superposition coding," *Opt. Exp.*, vol. 25, no. 24, pp. 29856-29863, 2017.
22. C. Chen, W. Zhong, H. Yang, P. Du, Y. Yang, "Flexible-Rate SIC-Free NOMA for Downlink VLC Based on Constellation Partitioning Coding," *IEEE Wireless Commun. Lett.*, vol. 8, no. 2, pp. 568-571, 2018.
23. X. Chen, M. Jiang, "Adaptive Statistical Bayesian MMSE Channel Estimation for Visible Light Communication", *IEEE Transactions on Signal Processing*, vol. 65, no. 5, pp. 1287 – 1299, 2017.
24. K. Reddy Sekhar, R.Mitra, "MBER Combining for MIMO VLC With User Mobility and Imperfect CSI", *IEEE Communications Letters*, vol. 24, no. 2, pp. 376-380, 2020.
25. Y. Wang, X. Huang, L. Tao, J. Shi, and N. Chi, "4.5-Gb/s RGB-LED based WDM visible light communication system employing CAP modulation and RLS based adaptive equalization," *Opt. Exp.*, vol. 23, no. 10, pp. 13626–13633, 2015.
26. N. Chi, M. Zhang, Y. Zhou, and J. Zhao, "3.375-Gb/s RGB-LED based WDM visible light communication system employing PAM-8 modulation with phase shifted Manchester coding," *Opt. Exp.*, vol. 24, no. 19, pp. 21663–21673, 2016.
27. G. Stepniak, J. Siuzdak, and P. Zwierko, "Compensation of a VLC phosphorescent white LED nonlinearity by means of Volterra DFE," *IEEE Photonics Technol. Lett.*, vol. 25, no. 16, pp. 1597–1600, 2013.
28. S. Liang, Z. Jiang, L. Qiao, X. Lu, and N. Chi, "Faster-Than-Nyquist precoded CAP modulation visible light communication system based on nonlinear weighted look-up table predistortion," *IEEE Photonics J.* vol. 10, no. 1, pp. 1–9, 2018.
29. R. Mitra, V. Bhatia, "Precoded Chebyshev-NLMS-Based Pre-Distorter for Nonlinear LED Compensation in NOMA-VLC," *IEEE Transactions on Communications*, vol. 65, no. 11, pp. 4845–4856, Nov. 2017.
30. X. Lu, K. Wang, L. Qiao, W. Zhou, Y. Wang, and N. Chi, "Non-linear compensation of multi-cap VLC system employing clustering algorithm-

based perception decision," *IEEE Photonics Journal*, vol. 9, no. 5, pp. 1-9, 2017.

31. Jie Ma, Jing He, Jin Shi, Jing He, Zhihua Zhou, Rui Deng, "Nonlinear Compensation Based on K-Means Clustering Algorithm for Nyquist PAM-4 VLC System," *IEEE Photonics Technology Letters*, vol. 31, no. 12, pp. 935-938, 2019.

32. X. Lu, C. Lu, W. Yu, L. Qiao, S. Liang, A. P. T. Lau and N. Chi, "Memory-controlled deep LSTM neural network post-equalizer used in high-speed PAM VLC system," *Opt. Exp.*, vol. 27, no. 5, pp. 7822–7833, 2019.

33. Hoon Lee, Inkyu Lee, and Sang Hyun Lee, "Deep learning based transceiver design for multi-colored VLC systems," *Opt. Exp.*, vol. 26, no. 5, pp. 6222-6238, 2018.

34. Shuai Ma, Jiahui Dai, Songtao Lu, Hang Li, Han Zhang, Chun Du, Shiyin Li, "Signal Demodulation with Machine Learning Methods for Physical Layer Visible Light Communications: Prototype Platform, Open Dataset, and Algorithms," *IEEE Access*, vol. 7, pp. 2169-3536, 2019.

35. Monica Bianchini and Franco Scarselli, "On the Complexity of Neural Network Classifiers: A Comparison Between Shallow and Deep Architectures", *IEEE Transactions on Neural Networks and Learning Systems*, vol. 25, no. 8, pp. 1553-1565, 2014.

36. By Alex Krizhevsky, Ilya Sutskever, and Geoffrey E. Hinton, "ImageNet Classification with Deep Convolutional Neural Networks", *Communications of the ACM*, vol. 60, no. 6, pp. 84-90, 2017.

37. Lilin Yi, Tao Liao, Luyao Huang, Lei Xue, Peixuan Li, Weisheng Hu, "Machine Learning for 100 Gb/s/λ Passive Optical Network", *Journal of Lightwave Technology*, vol. 37, no. 6, pp. 1621 – 1630, 2019.

38. X. Guan, Qing Yang, and Chun-Kit Chan, "Joint Detection of Visible Light Communication Signals Under Non-Orthogonal Multiple Access", *IEEE Photonics Technology Letters*, vol. 29, no. 4, pp. 377-380, 2017